12-18-2014

Electrostatic Force Microscopy and Electrical Isolation of Etched Few-Layer Graphene Nano-Domains

D. Patrick Hunley
University of Kentucky, patrickhunley@uky.edu

Abhishek Sundararajan
University of Kentucky, abhishek.s@uky.edu

Mathias J. Boland
University of Kentucky, mathias.boland@uky.edu

Douglas R. Strachan
University of Kentucky, doug.strachan@uky.edu

Electrostatic force microscopy and electrical isolation of etched few-layer graphene nano-domains

D. Patrick Hunley, Abhishek Sundararajan, Mathias J. Boland, and Douglas R. Strachan[a)]
Department of Physics and Astronomy, University of Kentucky, Lexington, Kentucky 40506, USA

(Received 13 August 2014; accepted 7 December 2014; published online 18 December 2014)

Nanostructured bi-layer graphene samples formed through catalytic etching are investigated with electrostatic force microscopy. The measurements and supporting computations show a variation in the microscopy signal for different nano-domains that are indicative of changes in capacitive coupling related to their small sizes. Abrupt capacitance variations detected across etch tracks indicates that the nano-domains have strong electrical isolation between them. Comparison of the measurements to a resistor-capacitor model indicates that the resistance between two bi-layer graphene regions separated by an approximately 10 nm wide etch track is greater than about $1 \times 10^{12}\,\Omega$ with a corresponding gap resistivity greater than about $3 \times 10^{14}\,\Omega \cdot$ nm. This extremely large gap resistivity suggests that catalytic etch tracks within few-layer graphene samples are sufficient for providing electrical isolation between separate nano-domains that could permit their use in constructing atomically thin nanogap electrodes, interconnects, and nanoribbons. © *2014 AIP Publishing LLC*. [http://dx.doi.org/10.1063/1.4904709]

Few-layer graphene (FLG) is an atomically thin material having many beneficial properties, such as high carrier mobility, high thermal conductivity, and tremendous strength, which make it a potentially useful material for future nanoscale devices and integrated circuits.[1–7] To achieve this goal of utilizing FLG in nano-electronics requires the ability to construct nanoscale structures out of it.[8] To date, there have been a number of approaches investigated to achieving nanoscale FLG.[9–26] One such approach which has received attention is the catalytic etching of few-layer graphene.[27] This catalytic etching has long been known to result in crystallographically defined etched domains and tracks in bulk graphite.[28] It has recently been found that many of the remarkable etch patterns obtained within bulk graphite persist to the FLG domain as well[27]—even when the films are supported on amorphous insulating substrates.[27,29] The fact that the crystallographic etch patterns can be obtained on insulating substrates indicates that catalytic etching could be a way to construct nanoscale electrically isolated FLG segments useful for devices. While there have been a number of investigations probing the electrical properties of nanostructured FLG,[14,15,30–32] further measurements are required to understand and assess the effects of nanoscale processing and confinement. This is particularly true for nanoscale FLG obtained through catalytic etching that can be difficult to probe due to the close proximity of the nanoscale domains.

Here, we use electrostatic force microscopy (EFM) to investigate catalytically etched bi-layer graphene samples. EFM has recently been used to probe variations of the surface potential of FLG as its thickness varies.[33] In contrast to this previous work, we find an EFM signal that varies significantly between nanoscale FLG domains even though they have the same thickness. We obtain evidence that the change in the EFM response is due to changes in the capacitive coupling as the size of the nanoscale FLG domains is reduced. Furthermore, the fact that the EFM signal changes abruptly in going between adjacent domains gives a lower-bound estimate of their electrical isolation.

The catalytically etched graphene samples used in this investigation were prepared through mechanical exfoliation onto p^+-doped silicon substrates having a 300 nm thermal oxide layer,[34,35] followed by processing in a chemical vapor deposition (CVD) furnace.[27,29] In the investigation that follows, we focus in detail on a region of the sample containing

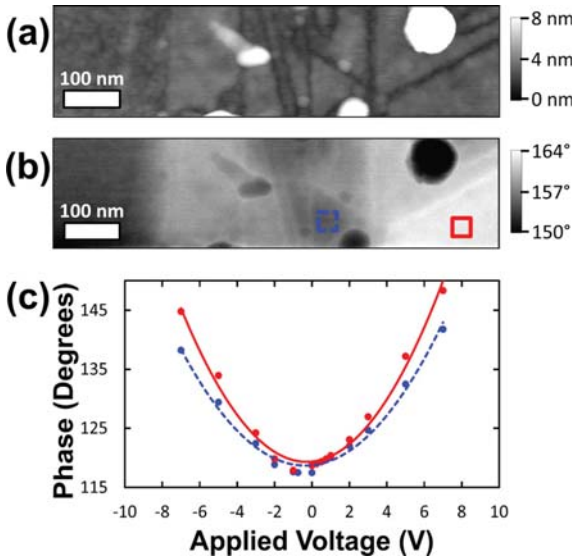

FIG. 1. (a) Atomic force microscope topography image of a bi-layer graphene (light grey) sample which has been catalytically etched with Ni nanoparticles. The etch tracks down to the insulating SiO_2 are the darker lines, the round white regions are catalyst particles, and the left region is exposed SiO_2 substrate. (b) EFM image of the same region taken at constant 7 V that shows a signal varying for different etched domains. (c) Spatial averages of the signals within the solid and dashed boxes in (b) at varying applied tip voltages with quadratic fits. The solid and dashed fits to the data in (c) correspond to the respective solid and dashed boxed regions in (b).

[a)]Email: doug.strachan@uky.edu

only etch tracks with negligible amounts of carbon nanotubes grown on top of the FLG.[29,36,37]

We start with a bi-layer region (as shown in Fig. 1(a)) that has considerable etching and appears, according to AFM, to have several electrically isolated regions. The EFM method we utilize is a two-pass technique consisting of a conducting tip where the first obtains the topography and the second retraces the topography a fixed height of 36 nm above the surface.[35] During the second pass, the cantilever is driven close to resonance using the dithering piezo with a fixed applied bias between the tip and the doped Si back-gate substrate, while the phase shift of the driven cantilever is measured. Figure 1(b) shows such an EFM phase image acquired with a 7 V tip-substrate bias of the same etched bi-layer region, as shown in Fig. 1(a). This image clearly shows that the various bi-layer regions have very different phase shifts for a constant bias. This difference in EFM response between electrically isolated bi-layer regions is further demonstrated by investigating the phase response as a function of bias. Figure 1(c) shows such a comparison of the phase versus bias for the two regions within the square blocks in Fig. 1(b). Both regions show a parabolic phase response having their minima located at the same bias but with different concavities. This EFM behavior is distinct from previous measurements over multilayer graphene which, in contrast, show a constant concavity for such phase plots, but with minima that occur at varying voltages depending on the few-layer-graphene thickness.[33]

The EFM measurements can be understood by approximating the cantilever response as due to a total capacitance (C_T), a surface potential (φ_S), an applied electrochemical potential to the tip relative to back-gate (V_{app}), and a work function difference between the tip and back-gate (ΔW). This provides a force gradient for the tip as a function of its vertical height (z) above the sample that alters the cantilever's resonance frequency.[38] For a cantilever driven at a fixed frequency near its resonance above a conducting sample surface, the change in the oscillatory phase is related to the force gradient through

$$\Delta\varphi \cong \frac{Q}{k}F'(z_0) = \frac{Q}{2k}(V_{app} - \varphi_S - \Delta W)^2 C_T''(z_0), \quad (1)$$

where Q is the oscillator quality factor and k is the effective spring constant. For large-area graphene samples, which are relevant to the experiments in Ref. 33, the only term which varies appreciably for a constant tip-FLG height and tip material is the surface potential of the FLG which depends on its thickness. This results in nearly identical parabolic phase curves as a function of potential which are displaced according to the varying surface potential of the FLG,[33] in agreement with Eq. (1).

For the samples considered here, where all the FLG segments are bi-layer, the surface potential is relatively constant for the etched domains, and thus the phase-shift parabolas should all have the same voltage minima. However, different lateral positions above the sample should result in a variation of $C_T''(z_0)$ due to differences in the capacitive coupling to the geometrically varying shapes of etched FLG below. This should result in parabolic phase-shift curves with different curvatures but with minima located at the same voltage, like those shown in Fig. 1(c). Since the electrical coupling is strongest between the tip and the FLG directly below it, the geometry of this closest etched domain should make the greatest contribution to the curvature of the phase parabola. Evidence that this effect is the source of the different phase responses observed in Figs. 1(b) and 1(c) is obtained by plotting the quadratic fitting coefficients of the EFM parabolas as a function of the surface area of the graphene segments below the tip, as shown in Fig. 2.

To understand this variation of the quadratic EFM response as a function of area, we have performed finite-element simulations of a tip over various geometrical arrangements of conducting sheets. The simulations were performed with a cylindrically symmetric arrangement where the tip is located along the central vertical axis of the computational volume, given by a cylinder of height 5300 nm and radius 2820.95 nm. The cylindrical symmetry allows for the simulation of the fields within the entire volume to be simplified to that of a two-dimensional slice that significantly increases the speed and precision of the computations. A back conducting plane is placed on the lower surface of the cylindrical space with various arrangements of FLG domains located 300 nm above it, as seen in the vicinity of the tip in Fig. 3(a). The simulated conducting tip is given a total height of 4260 nm, a realistic radius of curvature of 25 nm and conical opening angle (as measured from the central axis) of 25°, and its end is located a lift height z above the plane containing the FLG domains.

The first arrangement we consider consists of a single FLG domain of a specified area separated with a single 10 nm gap from a continuous larger surrounding domain with an outside radius of 2251 nm. The dotted-dashed line in Figure 3(b) is the potential distribution along the radial direction of the FLG plane for a tip height of 36 nm resulting in a significant voltage drop across the 10 nm gap. By performing simulations at various tip heights from 32 to 40 nm we are able to estimate C_T'' at $z_0 = 36$ nm. The top dot-dashed curve in Fig. 3(c) shows the results of such a computation as a function of the inner FLG domain area. While there is a clear dependence of C_T'' on area, the 4.30% change over this range,

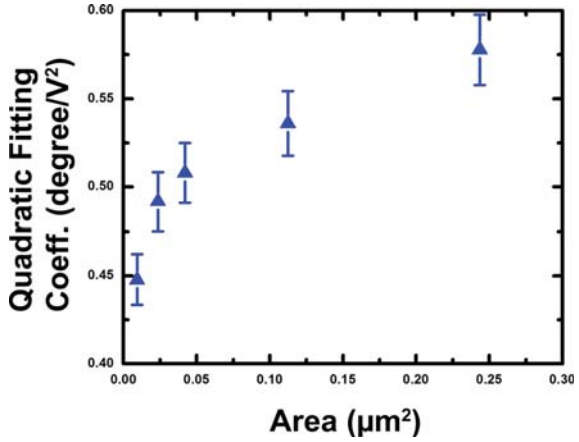

FIG. 2. The quadratic fitting coefficient of the EFM phase curves plotted against the surface area of the bi-layer graphene domain size directly below the tip (error bars estimated from fits).

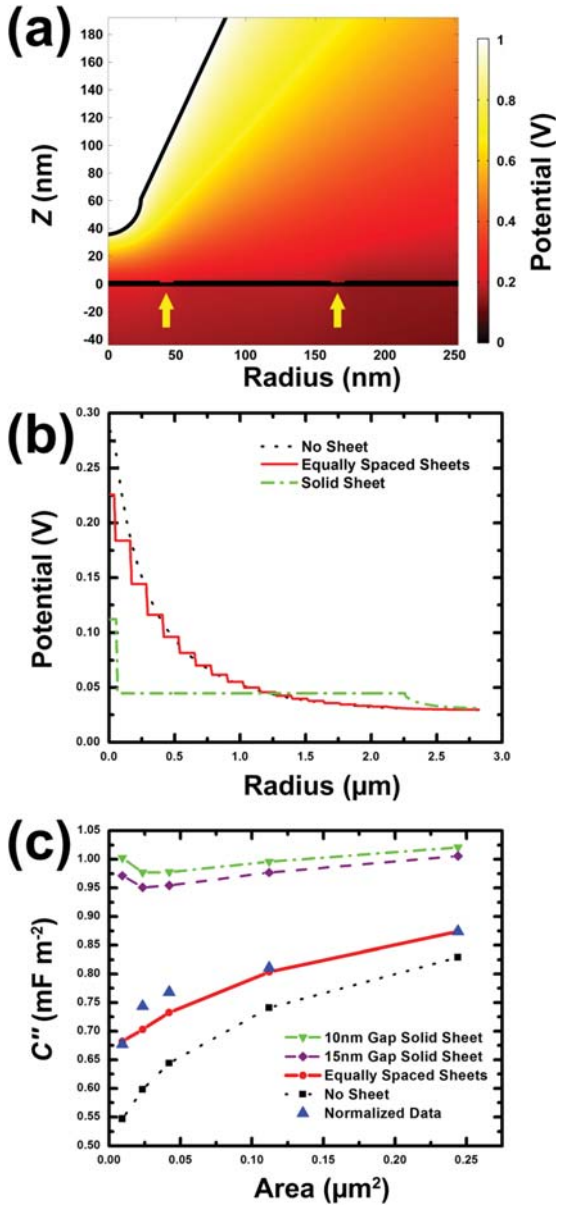

FIG. 3. Finite element simulations of the electrostatic interactions between the EFM tip and the etched FLG sample. (a) Cross-sectional slice of the simulation in the vicinity of the tip with etched FLG located on the plane $z = 0$. Arrows point to etch tracks and a conducting plane exists at $z = -300$ nm. (b) The potential on the plane $z = 0$ for various FLG arrangements with central one of radius 54.4 nm. "No Sheet" does not have additional FLG, "Solid Sheet" has a single surrounding FLG sheet separated with a 10 nm gap and an outside radius of 2251 nm, and "Equally Spaced Sheets" has a series of FLG rings of width 113 nm each separated by 10 nm. (c) C_T'' determined by the simulations as a function of the area of the domain directly below the tip. The experimental data from Fig. 2 are plotted on this curve with a single scaling factor.

defined as $(C''_{Tmax} - C''_{Tmin})/C''_{Tmax}$, is not sufficient to account for the 22.5% change we observe in our measurements. This discrepancy does not appear to be due to a variation in etch track width, as the use of a 15 nm gap (which is larger than the size determined experimentally through AFM) in the calculations has only a minimal affect on the results, as seen by the dashed line in Fig. 3(c). In contrast, computations without an outside FLG sheet show a 34.0% change of C_T'' over the same range of areas (plotted as the dotted curve in Fig. 3(c)), which is even greater than experimentally observed. This suggests that the FLG not directly below the tip affects the overall capacitance to an intermediate level between these two extreme scenarios. Direct support for this is obtained by simulating the surrounding etched FLG regions as concentric circular sheets of width 113 nm (i.e., a typical size for an etched domain in these samples) spaced by 10 nm gaps. This results in a 22.0% change of C_T'' shown by the solid red line in Fig. 3(c) that is in good agreement with the measured data (plotted as the blue triangles). A radial plot of the potential on the graphene surface for this intermediate scenario (the solid line in Fig. 3(b)) shows a series of drops at the etched gaps that are largest close to the tip and that approach the profile without an outside sheet (the black dotted line) away from the tip. This suggests that the domain geometry not directly below the tip gives a non-negligible contribution to the EFM measurements. The scatter of the experimental data off of the simulated curve in Fig. 3(c) is likely due to variation in these nearby FLG domain arrangements not directly below the tip. Future experiments using coaxial EFM tips[39] might make it possible to shield the capacitive coupling to only the single closest etched FLG domain.

In the above simulations of C_T'', we have ignored effects due to the cantilever itself which can be important in EFM force measurements.[40,41] This is justified in our EFM force gradient measurements, as is seen by using a parallel-plate approximation for the cantilever,[42] where its width ($W = 28\,\mu$m), length ($L = 225\,\mu$m), and tip height ($h = 17\,\mu$m) are inserted into $C_{cant} = WL\epsilon_0/h$, $C'_{cant} \sim -\frac{WL\epsilon_0}{h^2} = -1.93 \times 10^{-10}$ F/m, and $C''_{cant} \sim 2WL\epsilon_0/h^3 = 2.27 \times 10^{-5}$ F/m^2. Although this C'_{cant} has a larger magnitude than the one we simulate, the estimate of C''_{cant} is only ~3% of the value we compute, and can thus be neglected in the force gradient EFM measurements. In addition, our simulations only take the geometrical aspects of the capacitive coupling in the EFM measurements into account, and neglect the local surface potential. For large area FLG films that provide a surface with a nearly constant surface potential (like in the previous EFM measurements of FLG[33]) the minimum of the phase parabola should directly reflect the surface potential. In contrast, when the size of the FLG conducting region is small enough such that the tip appreciably couples directly to the back conducting plane, the phase minimum will not in general be directly related to the surface potential of the conducting FLG film.

The fact that the EFM phase response changes abruptly for adjacent etched bi-layer graphene segments in Fig. 1 permits a lower estimate of the resistive barriers provided by the etch tracks. For the etched system to act as electrically separated conducting FLG domains that maintain the voltage drops seen in Fig. 3(b), the resistance between them must be large enough to prevent their electrical equilibration over the time scale probed by EFM. Thus, the *RC* time scale for electrical equilibration must be greater than the characteristic EFM probing time (τ) of the experiments as represented by the simplified two-capacitor circuit model in Fig. 4. In this model, the EFM probe is positioned over the first FLG domain (G_1) such that the tip only appreciably couples to it. An adjacent etched domain (G_2) having an overall different capacitive coupling to the environment is connected to G_1

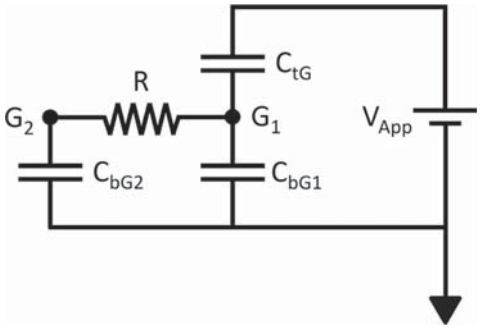

FIG. 4. A simplified circuit diagram that approximates the electrostatic force microscopy measurement when the tip is over one nano-domain (G_1) and is separated by an etch track to another domain (G_2). In the model, the tip-graphene capacitance to a domain is C_{tG}, the two capacitances to the environment are C_{bG1} and C_{bG2}, and the parasitic conductance between the two domains is represented by the resistor R.

through possible parasitic residual conductance across the etch tracks. Using this model, it can be shown that when either the scan time (the time over which the tip is located above a particular domain) or the oscillation time of the cantilever is less than the RC equilibration time that abrupt changes in EFM signal are possible in switching the location of the tip between G_1 and G_2.[35] To obtain a lower-bound of the etch-track resistance, we use the shortest of these scales, which is the oscillation time and is given by $\tau = 2\pi/\omega_0$, where ω_0 is the resonance frequency of the 67.461 kHz probes. The capacitance of a domain consisting of an outside perimeter of $l = 342$ nm is estimated as 1.41×10^{-17} F by using the simulations discussed above in Fig. 3 consisting of equally spaced sheets. The resistance between etched segments is given by $R = \rho_{gap}/l$, where ρ_{gap} is the resistivity of the gap (and not a bulk resistivity despite the similar units) which yields the entire resistance across it when divided by its length, l. A lower-bound to the gap resistivity can therefore be estimated from the RC time-constant using the above values to obtain $\rho_{gap} \gtrsim l\tau/C = 3 \times 10^{14}\,\Omega \cdot \text{nm}$. This extremely large gap resistivity indicates that the samples we have synthesized yield electrically isolated bi-layer regions.

In conclusion, we have made an EFM investigation of nanostructured bi-layer graphene samples that are formed by catalytic etching along narrow (approximately 10 nm wide) tracks. The measurements show a variation in the quadratic term of the EFM phase signal for different nano-domains of bi-layer graphene. Quantitative comparison to simulations indicates that the change in quadratic behavior is due to a decrease in the second derivative of the overall capacitive coupling as the closest nano-domain becomes smaller. The fact that abrupt capacitance variations can be measured across etch tracks indicates that the nano-domains have strong electrical isolation. Modeling the system as a RC circuit permits a lower estimate of the electrical isolation between etched nano-domains. This calculation gives a lower-bound estimate to the gap resistivity of $3 \times 10^{14}\,\Omega \cdot \text{nm}$ between two bi-layer graphene regions separated by an approximately 10 nm wide etch track. This extremely large gap resistivity suggests that catalytic etch tracks within FLG samples are sufficient for providing electrical isolation between separate nano-domains that could permit their use in constructing atomically thin nanogap electrodes,[22,25,43] interconnects,[30,32] and nanoribbons.[14,31]

The work was supported in part by the National Science Foundation (NSF) through Grant No. DMR-0805136, the Kentucky NSF EPSCoR program through Award No. EPS-0814194, the University of Kentucky (UK) Center for Advanced Materials (CAM), a grant from the Kentucky Science and Engineering Foundation as per Grant/Award Agreement No. KSEF-2928-RDE-016 with the Kentucky Science and Technology Corporation, and a Research Support Grant from the University of Kentucky Office of the Vice President for Research.

[1]A. K. Geim and K. S. Novoselov, "The rise of graphene," Nat. Mater. **6**, 183–191 (2007).
[2]X. Jia, J. Campos-Delgado, M. Terrones, V. Meunier, and M. S. Dresselhaus, "Graphene edges: A review of their fabrication and characterization," Nanoscale **3**, 86–95 (2011).
[3]K. Nakada, M. Fujita, G. Dresselhaus, and M. S. Dresselhaus, "Edge state in graphene ribbons: Nanometer size effect and edge shape dependence," Phys. Rev. B **54**, 17954–17961 (1996).
[4]M. H. D. Guimaraes, O. Shevtsov, X. Waintal, and B. J. van Wees, "From quantum confinement to quantum hall effect in graphene nanostructures," Phys. Rev. B **85**, 075424 (2012).
[5]Y.-W. Son, M. L. Cohen, and S. G. Louie, "Half-metallic graphene nanoribbons," Nature **444**, 347–349 (2006).
[6]Y.-W. Son, M. L. Cohen, and S. G. Louie, "Energy gaps in graphene nanoribbons," Phys. Rev. Lett. **97**, 216803 (2006).
[7]V. Barone, O. Hod, and G. E. Scuseria, "Electronic structure and stability of semiconducting graphene nanoribbons," Nano Lett. **6**, 2748–2754 (2006).
[8]A. K. Geim and A. H. MacDonald, "Graphene: Exploring carbon flatland," Phys. Today **60**(8), 35–41 (2007).
[9]E. Cruz-Silva, A. R. Botello-Mendez, Z. M. Barnett, X. Jia, M. S. Dresselhaus, H. Terrones, M. Terrones, B. G. Sumpter, and V. Meunier, "Controlling edge morphology in graphene layers using electron irradiation: From sharp atomic edges to coalesced layers forming loops," Phys. Rev. Lett. **105**, 045501 (2010).
[10]X. Jia, M. Hofmann, V. Meunier, B. G. Sumpter, J. Campos-Delgado, J. M. Romo-Herrera, H. Son, Y.-P. Hsieh, A. Reina, J. Kong, M. Terrones, and M. S. Dresselhaus, "Controlled formation of sharp zigzag and armchair edges in graphitic nanoribbons," Science **323**, 1701–1705 (2009).
[11]Y. Lu, B. Goldsmith, D. R. Strachan, J. H. Lim, Z. Luo, and A. T. C. Johnson, "High-on/off-ratio graphene nanoconstriction field-effect transistor," Small **6**, 2748–2754 (2010).
[12]L. A. Ponomarenko, F. Schedin, M. I. Katsnelson, R. Yang, E. W. Hill, K. S. Novoselov, and A. K. Geim, "Chaotic dirac billiard in graphene quantum dots," Science **320**, 356–358 (2008).
[13]K. Kim, A. Sussman, and A. Zettl, "Graphene nanoribbons obtained by electrically unwrapping carbon nanotubes," ACS Nano **4**, 1362–1366 (2010).
[14]M. Y. Han, B. Ozyilmaz, Y. Zhang, and P. Kim, "Energy band-gap engineering of graphene nanoribbons," Phys. Rev. Lett. **98**, 206805 (2007).
[15]L. Y. Jiao, L. M. Xie, and H. J. Dai, "Densely aligned graphene nanoribbons at similar to 35 Nm pitch," Nano Res. **5**, 292–296 (2012).
[16]L. Y. Jiao, X. R. Wang, G. Diankov, H. L. Wang, and H. J. Dai, "Facile synthesis of high-quality graphene nanoribbons," Nat. Nanotechnol. **5**, 321–325 (2010).
[17]L. Jiao, L. Zhang, X. Wang, G. Diankov, and H. Dai, "Narrow graphene nanoribbons from carbon nanotubes," Nature **458**, 877–880 (2009).
[18]Y. Lu, C. A. Merchant, M. Drndic, and A. T. C. Johnson, "*In situ* electronic characterization of graphene nanoconstrictions fabricated in a transmission electron microscope," Nano Lett. **11**, 5184–5188 (2011).
[19]F. Borrnert, L. Fu, S. Gorantla, M. Knupfer, B. Buchner, and M. H. Rummeli, "Programmable sub-nanometer sculpting of graphene with electron beams," ACS Nano **6**, 10327–10334 (2012).
[20]M. D. Fischbein and M. Drndic, "Electron beam nanosculpting of suspended graphene sheets," Appl. Phys. Lett. **93**, 113107 (2008).
[21]J. Moser and A. Bachtold, "Fabrication of large addition energy quantum dots in graphene," Appl. Phys. Lett. **95**, 173506 (2009).

[22]B. Standley, W. Bao, H. Zhang, J. Bruck, C. N. Lau, and M. Bockrath, "Graphene-based atomic-scale switches," Nano Lett. **8**, 3345–3349 (2008).
[23]D. V. Kosynkin, A. L. Higginbotham, A. Sinitskii, J. R. Lomeda, A. Dimiev, B. K. Price, and J. M. Tour, "Longitudinal unzipping of carbon nanotubes to form graphene nanoribbons," Nature **458**, 872–876 (2009).
[24]J. M. Cai, P. Ruffieux, R. Jaafar, M. Bieri, T. Braun, S. Blankenburg, M. Muoth, A. P. Seitsonen, M. Saleh, X. L. Feng, K. Mullen, and R. Fasel, "Atomically precise bottom-up fabrication of graphene nanoribbons," Nature **466**, 470–473 (2010).
[25]F. Prins, A. Barreiro, J. W. Ruitenberg, J. S. Seldenthuis, N. Aliaga-Alcalde, L. M. K. Vandersypen, and H. S. J. van der Zant, "Room-temperature gating of molecular junctions using few-layer graphene nanogap electrodes," Nano Lett. **11**, 4607–4611 (2011).
[26]A. Narita, X. L. Feng, Y. Hernandez, S. A. Jensen, M. Bonn, H. F. Yang, I. A. Verzhbitskiy, C. Casiraghi, M. R. Hansen, A. H. R. Koch, G. Fytas, O. Ivasenko, B. Li, K. S. Mali, T. Balandina, S. Mahesh, S. De Feyter, and K. Mullen, "Synthesis of structurally well-defined and liquid-phase-processable graphene nanoribbons," Nat. Chem. **6**, 126–132 (2014).
[27]S. S. Datta, D. R. Strachan, S. M. Khamis, and A. T. Johnson, "Crystallographic etching of few-layer graphene," Nano Lett. **8**, 1912–1915 (2008).
[28]A. Tomita and Y. Tamai, "Optical microscopic study on the catalytic hydrogenation of graphite," J. Phys. Chem. **78**, 2254–2258 (1974).
[29]L. C. Campos, V. R. Manfrinato, J. D. Sanchez-Yamagishi, J. Kong, and P. Jarillo-Herrero, "Anisotropic etching and nanoribbon formation in single-layer graphene," Nano Lett. **9**, 2600–2604 (2009).
[30]A. D. Liao, J. Z. Wu, X. R. Wang, K. Tahy, D. Jena, H. J. Dai, and E. Pop, "Thermally limited current carrying ability of graphene nanoribbons," Phys. Rev. Lett. **106**, 256801 (2011).
[31]X. Wang, Y. Ouyang, X. Li, H. Wang, J. Guo, and H. Dai, "Room-temperature all-semiconducting sub-10-nm graphene nanoribbon field-effect transistors," Phys. Rev. Lett. **100**, 206803 (2008).
[32]Z. Chen, Y.-M. Lin, M. J. Rooks, and P. Avouris, "Graphene nano-ribbon electronics," Physica E **40**, 228–232 (2007).
[33]S. S. Datta, D. R. Strachan, E. J. Mele, and A. T. Johnson, "Surface potentials and layer charge distributions in few-layer graphene films," Nano Lett. **9**, 7–11 (2009).
[34]K. S. Novoselov, A. K. Geim, S. V. Morozov, D. Jiang, Y. Zhang, S. V. Dubonos, I. V. Grigorieva, and A. A. Firsov, "Electric field effect in atomically thin carbon films," Science **306**, 666–669 (2004).
[35]See supplementary material at http://dx.doi.org/10.1063/1.4904709 for details on sample preparation, scanning probe measurements, and a discussion on the relevant time scales for force gradient electrostatic force microscopy measurements.
[36]D. P. Hunley, S. L. Johnson, J. K. Stieha, A. Sundararajan, A. T. Meacham, I. N. Ivanov, and D. R. Strachan, "Crystallographically aligned carbon nanotubes grown on few-layer graphene films," ACS Nano **5**, 6403–6409 (2011).
[37]M. Nasseri, D. P. Hunley, A. Sundararajan, M. J. Boland, and D. R. Strachan, "Tuning between crystallographically aligned carbon nanotube growth and graphene etching," Carbon **77**, 958–963 (2014).
[38]D. Bonnell, *Scanning Probe Microscopy and Spectroscopy: Theory, Techniques, and Applications*, 2nd ed. (Wiley-VCH, Inc., 2001).
[39]K. A. Brown, K. J. Satzinger, and R. M. Westervelt, "High spatial resolution kelvin probe force microscopy with coaxial probes," Nanotechnology **23**, 115703 (2012).
[40]S. Guriyanova, D. S. Golovko, and E. Bonaccurso, "Cantilever contribution to the total electrostatic force measured with the atomic force microscope," Meas. Sci. Technol. **21**, 025502 (2010).
[41]H. O. Jacobs, P. Leuchtmann, O. J. Homan, and A. Stemmer, "Resolution and contrast in kelvin probe force microscopy," J. Appl. Phys. **84**, 1168–1173 (1998).
[42]O. Cherniavskaya, L. W. Chen, V. Weng, L. Yuditsky, and L. E. Brus, "Quantitative noncontact electrostatic force imaging of nanocrystal polarizability," J. Phys. Chem. B **107**, 1525–1531 (2003).
[43]M. Tsutsui and M. Taniguchi, "Single molecule electronics and devices," Sensors **12**, 7259–7298 (2012).